3-19-2004

Relativistic Kinetic Reconnection as the Possible Source Mechanism for High Variability and Flat Spectra in Extragalactic Radio Sources

C. H. Jaroschek
Max-Planck-Institut fur extraterrestrische Physik

H. Lesch
Max-Planck-Institut fur extraterrestrische Physik

R. A. Treumann
Dartmouth College

The Astrophysical Journal, 605:L9–L12, 2004 April 10

RELATIVISTIC KINETIC RECONNECTION AS THE POSSIBLE SOURCE MECHANISM FOR HIGH VARIABILITY AND FLAT SPECTRA IN EXTRAGALACTIC RADIO SOURCES

C. H. Jaroschek,[1,2] H. Lesch,[1,2] and R. A. Treumann[1,3]
Received 2003 September 17; accepted 2004 March 1; published 2004 March 19

ABSTRACT

We present the first synchrotron power spectra of a self-consistent kinetic reconnection scenario in the highly relativistic regime of a pair plasma. A fully electromagnetic relativistic particle-in-cell code is used to study the late-time evolution of kinetic magnetic reconnection at high resolution with a total ensemble of more than 10^8 particles. We show (1) the importance of the extremely dynamic late-time evolution of the reconnection region for the generation of nonthermal particles, (2) the efficient synchrotron emission by the accelerated fraction of particles, and (3) the application of the simulation results to pair-dominated active galactic nucleus core regions—the presumable origin of "light" jets. We conclude that collisionless kinetic reconnection in the relativistic regime is capable of explaining the enormous power output of $P \sim 10^{47}$ ergs s^{-1} in certain luminous intraday variable quasars and the extremely hard observed radio spectra of flat-spectrum radio quasars.

Subject headings: acceleration of particles — galaxies: active — radiation mechanisms: nonthermal

1. INTRODUCTION

Extragalactic radio sources like active galactic nuclei (AGNs) exhibit various observational features that are a challenge for the theoretical understanding of the underlying microphysics (see Urri & Padovani 1995 for a recent review on radio-loud AGNs). The extreme intraday variability of certain luminous quasars (Wagner 1998; Quirrenbach et al. 1992; Kellermann & Pauliny-Toth 1981) places tight limits on the time and length scales of the emission process. High luminosities with energy dissipation of up to 10^{51} ergs (Reeves et al. 2002; Protheroe 2003) and remarkably hard spectra with spectral index $s > -0.5$ in certain flat-spectrum radio quasars (Teräsranta et al. 2001) need to be powered by a violent process. A promising source mechanism is magnetic reconnection as a fundamental plasma process that dissipates magnetic energy and efficiently generates nonthermal particles (Di Matteo 1998; Birk, Crusius-Wätzel, & Lesch 2001). Collisionless reconnection in electron-ion plasma is suggested by observations from the Earth's magnetotail (Nagai et al. 1998) and has been extensively studied in kinetic simulations (Drake 2001; Pritchett 2001). These simulations revealed that collisionless reconnection proceeds "fast" on electron inertial length scales; i.e., the reconnection outflow takes place at speeds comparable to the Alfvén velocity $v_{\rm out} \sim v_{\rm A}$. Since in a pair plasma, kinetic reconnection efficiency is not limited by ion inertia, we here use the term fast magnetic reconnection (FMR). In this Letter, we address the synchrotron power spectra generated within the late-time evolution of FMR in a relativistic pair plasma. There is convincing observational evidence for the existence of pair-dominated "light" jets (Wardle et al. 1998; Hirotani et al. 2000; Lobanov & Zensus 2001). Internal jet conditions do not allow for significant pair production; hence, these light jets probe the plasma conditions in certain AGN core regions. Zenitani & Hoshino (2001) first investigated the generation of nonthermal particles in FMR in the relativistic regime of a pair plasma in a two-dimensional particle-in-cell (PIC) simulation. The simulations presented here are entirely self-consistent using a fully electromagnetic relativistic PIC code (Zeiler et al. 2002). Their results are applied to environment parameters expected for certain AGN core regions. We discuss the total synchrotron power output, spectral features within the reconnection X-zone especially with respect to the observed extremely flat radio spectra, and pitch-angle distributions. We conclude that FMR in the relativistic regime is a promising mechanism to explain the extremely energetic processes underlying the fundamental plasma physics of light-jet–dominated extragalactic radio sources as an alternative scenario to conventional shock-in-jet intrinsic models (Marscher, Gear, & Travis 1992).

2. SIMULATION MODEL

The pair plasma reconnection configuration is studied in two and a half dimensions with a massively parallelized PIC code (see Birdsall & Langdon 2000 for details on the PIC model) for a total number of 1.5×10^8 particles. A one-dimensional Harris configuration (Harris 1962) is initialized in the magnetic field $B(y) = B_0 \tanh[(y - L_y/2)/w_0]$ and density $n = n_0 \,\mathrm{sech}^2[(y - L_y/2)/w_0]$; B_0 is the asymptotic magnetic field far away from the current sheet, and n_0 is the current sheet density without background contributions. The Harris sheet width is set to $w_0 = 1.85d_0$. The simulation is performed in the x- y plane with total system size $L_x \times L_y = 816d_0 \times 102d_0$. Length scales are normalized to the electron inertial length $d_0 = c/\omega_{p0}$, with the plasma frequency $\omega_{p0} = (4\pi n_0 e^2/m)^{1/2}$. Time steps are given in units of the inverse electron gyrofrequency $\omega_{c0}^{-1} = mc/eB_0$. The index "0" indicates quantities evaluated at reference conditions B_0 and n_0. Dimensional values are calculated in § 3.2 for B_0, n_0 of a typical astrophysical source environment. A fractional background of 0.77% n_0 is added homogeneously over the entire simulation box. A high-resolution grid mesh with $nx \times ny = 4096 \times 512$ grid points is applied; n_0 corresponds to 1168 pairs per grid cell. Initially, particles are inserted in phase space according to an isotropic relativistic Maxwell-Juettner distribution $f(p) \propto p^2 \exp[\gamma(p)mc^2/kT_0]$, where p is the particle momentum, c the speed of light, γ relativistic energy, m particle rest mass, and $kT_0 = 100$ keV the initial thermal energy. The Alfvén velocity $v_{\rm A}$ is comparable to c. The Debye length is resolved better than three times. The total energy E is conserved

[1] Center for Interdisciplinary Plasma Science, Max-Planck-Institut für extraterrestrische Physik, Giessenbachstrasse Postfach 1603, Garching 85748, Germany; cjarosch@mpe.mpg.de, tre@mpe.mpg.de.
[2] Observatory of the Ludwig-Maximilians University, Scheinerstrasse 1, Munich 81679, Germany; lesch@usm.uni-muenchen.de.
[3] Department of Physics and Astronomy, Dartmouth College, 6127 Wilder Laboratory, Hanover, NH 03755.

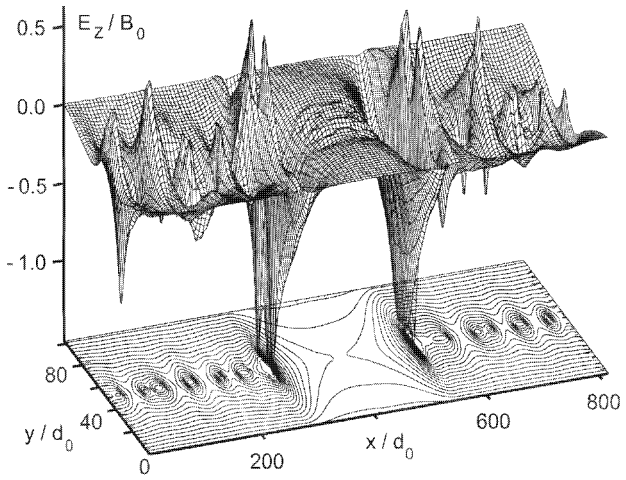

FIG. 1.—Composite plot of the acceleration electric field E_z (*meshed surface*) and the magnetic field line contours in the *x*-*y* simulation plane at $t\omega_{c0} = 220$. The first reconnection X-point is in the center; several secondary X-points evolve along the thin current sheet. Reconnection is responsible for $-E_z$ components. Superposed in the late-time stages are significant $-\boldsymbol{v}_x \times \boldsymbol{B}_y$ contributions that result from the merging of current sheet filaments.

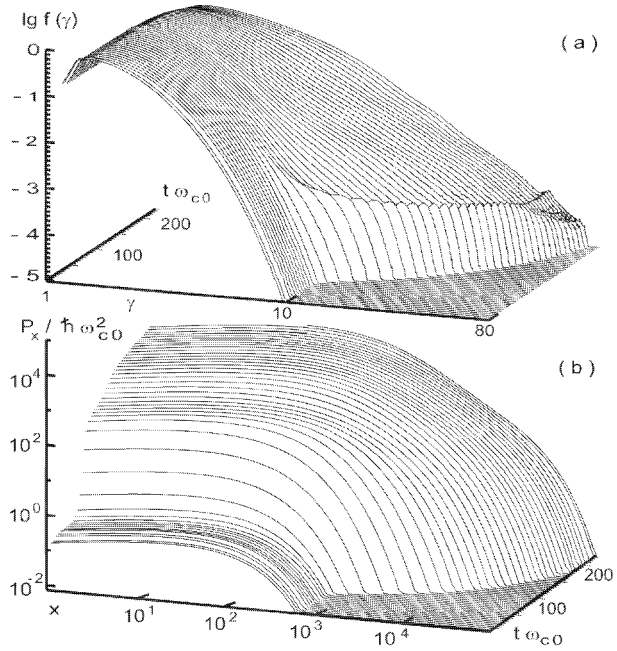

FIG. 2.—Double logarithmic stack plots of (*a*) the normalized particle distribution $f(\gamma)$ as a function of relativistic energy γ and (*b*) total spectral synchrotron power output $P(x)$ as a function of the dimensionless parameter $x = \omega/\omega_{c0}$. Simulation time is on the third axis. Reconnection onset at $t\omega_{c0} = 60$ coincides with the generation of nonthermal particles and significant synchrotron emission. The stability of the power-law tail in (*a*) is remarkable even in the highly dynamical late-time evolution of the system up to the cutoff at $\gamma \sim 68$. In (*b*), the cutoff frequency shifts by 2.5 powers of 10, and the frequency-integrated synchrotron power increases by a factor of 4.4×10^4.

within $\Delta E/E(t = 0) \sim 10^{-4}$ over the total simulation time of $t_{\rm tot}\omega_{c0} = 280$. Boundary conditions are periodic in *x* and *z*; the simulation is three-dimensional in momentum space. The *y*-boundary is open for particles and fields (Birdsall & Langdon 2000). The system configuration is similar to Zenitani & Hoshino (2001), with three important modifications. First, the system size is prolonged by a factor of 4 in the *x*- and by a factor of 2 in the *y*-direction. This extends the total simulated time by more than a factor of 3 and allows us to study the late-time evolution (Jaroschek et al. 2004) of the thin current sheet. Besides the initial reconnection X-point, several secondary X-points evolve. Particles are consecutively accelerated in various X-points, a phenomenon not observed by Zenitani & Hoshino (2001). Second, the nonperiodicity of the boundary condition in *y* allows us to consider a single Harris sheet configuration and hence to exclude the stabilizing effect of a neighboring current sheet. This causes a much more violent, highly nonlinear late-time evolution of the system. Third, an initial particle drift toward the centered X-point is pronounced, since the large *y*-extension of the system serves as a background particle reservoir, optimizing the efficiency of the particle acceleration mechanism, since reconnection rates are essentially limited by the inflow of magnetic flux carrying particles. Particle and field data at any given time step are used to calculate the synchrotron emission of the system. Contributions to the particle dynamics from radiative electric fields with frequencies beyond the grid mesh resolution are not an issue with respect to simulation self-consistency, since the typical synchrotron cooling time $t_{\rm sc}\omega_{c0} = 10^{12}/\gamma(B_0/1000\ {\rm G})^2 \sin^2\alpha$ exceeds the total simulation time by a factor of $t_{\rm sc}/t_{\rm tot} \sim 10^8$. The value γ denotes the accelerated particles' relativistic energy and α the pitch angle.

3. NUMERICAL RESULTS AND PHYSICAL PICTURE

3.1. *Nonthermal Particle Generation in the Late-Time Evolution*

Decisive for the efficiency of nonthermal particle generation is the reconnection rate, i.e., the inductive electric field E_z, and the time a particle remains within the X-zone (Zenitani & Hoshino 2001). Figure 1 shows the accelerating E_z-component and magnetic field line configuration for the late-time evolution at $t\omega_{c0} = 220$. The initial X-point is centered in the *x*-*y* plane. Several secondary X-points have evolved along the current sheet. In this extremely dynamic late stage, the current sheet filaments separated by the X-points tend to merge in the $\pm x$-direction, thereby generating additional accelerating E_z-fields via $-\boldsymbol{v}_x \times \boldsymbol{B}_y$ (Jaroschek et al. 2004); $\boldsymbol{v}_x$ is the merging speed of an individual current sheet filament and $\boldsymbol{B}_y$ the locally reconnected magnetic field strength. The dynamic contributions in the late-time evolution of the system superpose resonantly to $|E_z^{\rm max}/B_0| = 1.5$, compared to $|E_z^{\rm max}/B_0| = 0.33$ obtained by Zenitani & Hoshino (2001). High E_z-fields around X-points in close proximity make multiple acceleration in consecutive steps work efficiently (Jaroschek et al. 2004). The generation of nonthermal particles after reconnection onset is shown in the time evolution (Fig. 2*a*) of the normalized distribution function $f(\gamma)d\gamma$. Nonthermal contributions coincide with the formation of the initial X-point at $t\omega_{c0} = 60$. Zenitani & Hoshino (2001) found a power-law tail with a high-energy cutoff at $\gamma \sim 27$. In Figure 2*a*, $f(\gamma)d\gamma$ reaches up to $\gamma \sim 68$ during the late-time evolution. The cutoff energy finally is decisive for the total synchrotron power output as well as the cutoff frequency of the emission spectrum. Although the system is highly dynamic and the geometry of individual X-zones is more complicated, $f(\gamma)d\gamma$ still exhibits a power-law shape.

3.2. *Synchrotron Emission*

The time evolution of the total synchrotron power spectrum is shown in Figure 2*b*. Comparison with nonthermal particle generation in Figure 2*a* at $t\omega_{c0} = 60$ shows that reconnection onset and significant synchrotron power output dramatically co-

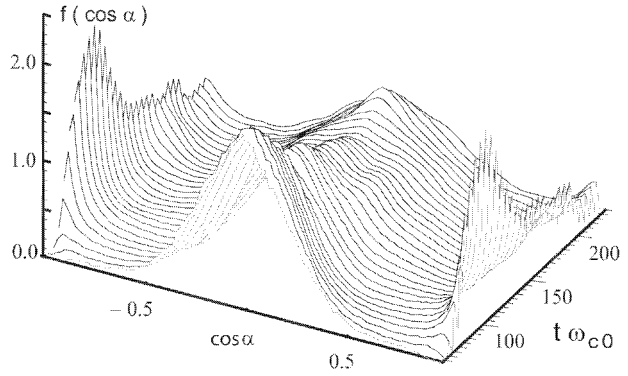

FIG. 3.—Time evolution of the pitch-angle distribution $f(\cos\alpha)$ starting with reconnection onset at $t\omega_{c0} = 60$. Perpendicular pitch angles dominate over all times. During an intermediate time phase, the first X-zone dominates and violent particle inflow at slightly oblique angles to the newly reconnected $\boldsymbol{B}_y$ component gives contributions at very small and very large pitch angles.

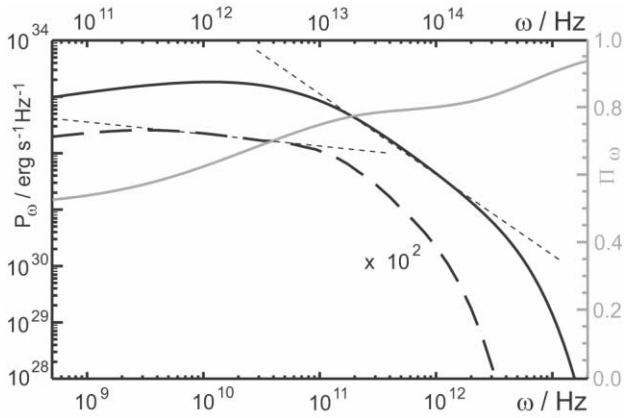

FIG. 4.—Total spectral synchrotron power output $P(\omega)$ as a function of frequency ω for typical environment parameters of a luminous extragalactic radio source. The value of $P(\omega)$ for the complete simulation box at $t\omega_{c0} = 220$ is represented by the solid black line (upper frequency axis). The dotted asymptote of the power-law tail exhibits a spectral index $s = -1.36$; the spectral cutoff reaches up into the optical. For the dashed black line, spectral emission $P(\omega)$ is spatially restricted to the first X-zone at $t\omega_{c0} = 135$; $P(\omega)$ is magnified by a factor of 10^2 to fit into the ordinate range. The spectrum is extremely flat with $s = -0.17$ in the frequency range 1 GHz $< \nu <$ 100 GHz. The emitted synchrotron emission (*solid black line*) is highly polarized, with spectral polarization $\Pi(\omega) > 75\%$ for $\omega > 10$ THz (*gray line, right axis*).

incide in time. From reconnection onset to the late evolution of the system, the integrated total synchrotron power increases by a factor of 4.4×10^4. There the cutoff frequency shifts by 2.5 powers of 10. Synchrotron pitch angles are dominated by particles moving perpendicular to the ambient field (Fig. 3). For $t\omega_{c0} < 60$, pitch angles are expected to be isotropic, but only initial thermal particles with $\omega_{\rm cut} > 10^{-8}\omega_{\rm cut,\,fin}$ of the final spectral cutoff $\omega_{\rm cut,\,fin}$ can contribute. At intermediate times, contributions from those particles appear that move just slightly oblique to $\boldsymbol{B}$. Certain luminous radio sources exhibit extreme intraday variability; i.e., the radiative flux doubles within a time window of $t_{\rm var} \lesssim 10^5$ s. This restricts the spatial extension of the emission region to $R < 10^{16}$ cm. Total bolometric luminosities of $P_{\rm tot} \sim 10^{47}$ ergs s^{-1} are measured. The total dissipated energy during such flaring events integrates up to $E_{\rm tot} = 10^{51}$ ergs; $P_{\rm tot}$ requires a $10^9\ M_\odot$ black hole accreting $M \sim 4.5\ M_\odot$ yr^{-1} at maximum Kerr efficiency close to the Eddington limit. Since we study pair plasma reconnection, the results apply to pair-dominated AGN core regions, which presumably serve as the "heads" of light jets. Plasma theoretical arguments yield jet head densities $n_0 = \dot{M}/\pi R^2 m v_{\rm jet} \sim 10^{10}$ cm^{-3} (Lesch, Appl, & Camenzind 1989) for jet velocities $v_{\rm jet} \sim c$ (Lobanov & Zensus 2001). The magnetic confinement of AGN coronal regions has been discussed by Rees (1987), who estimates the magnetic field strength to $B_0 \sim 0.4 f^{1/2}(P_{\rm tot}/10^{46}\ {\rm ergs\ s^{-1}})^{1/2}(R/10^{18}\ {\rm cm})^{-1} \sim 1000$ G; $f \sim 1$ is the fractional energy emitted by the central compact object as Poynting flux. The characteristic synchrotron cooling time $t_{\rm sc}$ is shorter than the dynamic timescales of the emission region. So a low-beta plasma is expected with plasma $\beta = 8\pi n_0 k T_0/B^2 \approx 0.1$–$0.01$. A typical temperature $T_0 \sim 10^9$ K is the consequence. Recent X-ray (Reeves et al. 2002) and radio (Protheroe 2003) data confirm the subequipartition argument as well as the values for n_0 and T_0. Under isotropic conditions, the emission ratio of synchrotron (S) to inverse Compton (IC) power $P_S/P_{\rm IC} = u_B/u_{\rm ph}$ in the Thomson limit is determined by the ratio of magnetic u_B to photon $u_{\rm ph}$ energy densities. Source luminosities $P_{\rm tot} \sim 10^{47}$ ergs s^{-1} imply $u_{\rm ph} \sim 10^3$ ergs cm^{-3} for isotropic emission out of core regions extending $R \sim 10^{16}$ cm. Consequently, for subequipartitioned coronal plasma synchrotron emission 10^{-2}–$10^{-3} \lesssim P_S/P_{\rm IC}$ dominates in the radio-optical regime. The corresponding time and length scales are $t_0 = \omega_{c0}^{-1} = 5.6 \times 10^{-11}(B_0/1000\ {\rm G})^{-1}$ s and $d_0 = 1.1(T_0/100\ {\rm keV}) \times (B_0/1000\ {\rm G})^{-1}(\beta/0.1)^{-1/2}$ cm, respectively. To relate the synchrotron power output of the microphysical plasma process with the synchrotron emission rate of a quasar, a stochastic distribution of reconnection zones over the entire coronal source region is assumed. Synchrotron self-absorption (SSA) and subsequent plasma "thermalization" effects (Ghisellini, Haardt, & Svensson 1998) are neglected. The dimensional scale height of the spectral synchrotron power is $P_0 = 2.5 \times 10^{27}(R/10^{16}d_0)^3(\mu/10^5)$ ergs s^{-1} Hz^{-1}. Spatial coherence limits of the emission region are constrained by $t_{\rm var}$; the further observational fact of constant radiative flux within a minimum time frame of $t_{\rm min} \sim 1$ ks places a condition on the temporal coherence of the emission event, accounted for in the event multiplicity μ. For the parameters at hand, an individual reconnection event takes place within $t_{\rm tot} \sim 10^{-8}$ to 10^{-7} s, which allows for a superposed cascade of $\sim 10^5$ events within 1 ks. This implies the very conservative assumption that the process, restoring the magnetic energy in the accretion disk corona, is 10^5 times slower than the respective dissipation process. In cooler environments ($T_0 \sim 10$ keV) and higher magnetic fields, the reconnection event gets even more confined, and the radiation output is even more violent. The typical synchrotron cooling time for such a source is $t_{\rm sc} = 10^2/\gamma_0(B_0/1000\ {\rm G})^2 \sim 0.1$–$10$ s. Hence, $t_{\rm tot} \ll t_{\rm sc} \ll t_{\rm var}$ assures the self-consistency of the simulation. According to the pitch-angle distributions (Fig. 3), perpendicular emission dominates, i.e., is at maximum efficiency. Figure 4 shows the late-time total synchrotron power spectrum at $t\omega_{c0} = 220$. With $B_0 = 1000$ G, $T_0 = 100$ keV, and $\beta = 0.1$, the spectrum exhibits a power law with spectral index $s = -1.4$ well up to the cutoff frequency at $\omega_{\rm cut} \sim 10^{15}$ Hz. The frequency-integrated total power output is $P_{\rm tot} = 3.5 \times 10^{46}$ ergs s^{-1}. If we restrict the source region to an individual X-point, extremely hard spectra result with $s = -0.17$ up to the cutoff frequency at $\nu_{\rm cut} \sim 100$ GHz. This intense synchrotron emission provides a plasma-theoretical foundation for recently observed extremely hard spectra from flat-spectrum radio sources with $s > -0.5$ in the frequency band 1.4 GHz $< \nu <$ 4.85 GHz by Teräsranta et al. (2001). We note that the hard radio spectra are independent of the time variability argument and hence are not restricted to AGN core regions. The values of P_0 and $\nu_{\rm cut}$ will vary according to B_0, n_0 present, for instance, in the jet, whereas

the power-law index remains invariant. Lobanov & Zensus (2001) identified a complex magnetic field structure in the jet, suggesting that magnetic reconnection is present. The synchrotron emission is highly polarized with polarization degree $\Pi(\omega) > 75\%$ beyond $\omega \sim 10$ THz. We note that this is the theoretical polarization for an individual reconnection zone, and the polarization degree decreases for a stochastic distribution of reconnection regions. Nevertheless, these results can in principle explain observed polarization degrees $\Pi(\omega = 3.67\ \mathrm{GHz}) = 60\%$–$70\%$ in jet components of BL Lac objects as well as $\Pi(\omega = 3.67\ \mathrm{GHz}) = 2\%$–$9\%$ (Gabuzda & Cawthorne 2000) in the respective core regions.

4. SUMMARY AND CONCLUSIONS

We calculated synchrotron emission spectra from self-consistent PIC simulations of FMR in the relativistic regime of a pair plasma. The highly dynamic nonlinear late-time evolution of a thin current sheet serves as the fundamental plasma scenario to obtain synchrotron power spectra for environment parameters expected in certain pair-dominated AGN core regions. We assumed strong magnetic confinement and neglected SSA. Particle distributions are highly nonthermal, which results in a dominant synchrotron spectral component. This deviates from models of thermal synchrotron emission (Wardziński & Zdziarski 2000). Observations of dominant X-/γ-ray emission via Comptonization exist (Reeves et al. 2002; Kubo et al. 1998). A more sophisticated study should clarify the importance of SSA/IC upscattering of ambient photons as a function of the density profile and isotropy deviations—especially with respect to blazar-type AGNs, in which synchrotron self-Comptonization becomes significant (Kino, Takahara, & Kusunose 2002). In the FMR scenario, the generation of nonthermal particles in an individual reconnection X-zone is confined to an extremely small volume of m^3 size and takes place on submicrosecond timescales for typical source environment parameters. This results in optimized spatial and temporal coherence as a consequence of high event multiplicity. Typical synchrotron cooling times range on the order of seconds. Hence, simulation self-consistency is not limited by the grid mesh resolution. We conclude that the synchrotron emission scenario presented here provides a satisfactory description of the energetics for the immense power output of $P_{\mathrm{tot}} \sim 10^{47}$ ergs s^{-1} and intraday radio variability within the constraints of an intrinsic AGN variability model. Hence, FMR is an alternative to shock-in-jet variability scenarios and is superior with respect to self-consistent generation of power-law spectra on the plasma kinetic level.

The original version of the PIC code was developed by A. Zeiler. The computations were performed on the IBM SP Power 4 system at the Computing Center of the Max-Planck-Society in Garching, Munich, and the HITACHI SR8000-F1 supercomputer of the Leibniz Computing Center, Munich.

REFERENCES

Birdsall, C. K., & Langdon, A. B. 2000, Plasma Physics via Computer Simulation (Bristol: IOP)
Birk, G. T., Crusius-Wätzel, A. R., & Lesch, H. 2001, ApJ, 559, 96
Di Matteo, T. 1998, MNRAS, 299, L15
Drake, J. F. 2001, Nature, 410, 525
Gabuzda, D. C., & Cawthorne, T. V. 2000, MNRAS, 319, 1056
Ghisellini, G., Haardt, F., & Svensson, R. 1998, MNRAS, 297, 348
Harris, E. G. 1962, Nuovo Cimento, 23, 15
Hirotani, K., Iguchi, S., Kimura, M., & Kiyoaki, W. 2000, ApJ, 545, 100
Jaroschek, C. H., Treumann, R. A., Lesch, H., & Scholer, M. 2004, Phys. Plasmas, 11, 1151
Kellermann, K. I., & Pauliny-Toth, I. K. 1981, ARA&A, 19, 373
Kino, M., Takahara, F., & Kusunose, M. 2002, ApJ, 564, 97
Kubo, H., Takahashi, T., Madejski, G., Tashiro, M., Makano, F., Inoue, S., & Takahara, F. 1998, ApJ, 504, 693
Lesch, H., Appl, S., & Camenzind, M. 1989, A&A, 225, 341
Lobanov, A. P., & Zensus, J. A. 2001, Science, 294, 128
Marscher, A. P., Gear, W. K., & Travis, J. P. 1992, in Variability of Blazars, ed. E. Valtaoja & M. Valtonen (Cambridge: Cambridge Univ. Press), 85
Nagai, T., et al. 1998, J. Geophys. Res., 103, 4419
Pritchett, P. L. 2001, J. Geophys. Res., 106, 3783
Protheroe, R. J. 2003, MNRAS, 341, 230
Quirrenbach, A., et al. 1992, A&A, 258, 279
Rees, M. J. 1987, MNRAS, 228, 47P
Reeves, J. N., Wynn, G., O'Brien, P. T., & Pounds, K. A. 2002, MNRAS, 336, L56
Teräsranta, H., Urpo, S., Wiren, S., & Valtonen, M. 2001, A&A, 368, 431
Urri, C. M., & Padovani, P. 1995, PASP, 107, 803
Wagner, S. J. 1998, in ASP Conf. Ser. 144, Radio Emission from Galactic and Extragalactic Compact Sources, ed. J. A. Zensus, G. B. Taylor, & J. M. Wrobel (San Francisco: ASP), 257
Wardle, J. F. C., Homan, D. C., Ojha, R., & Roberts, D. H. 1998, Nature, 395, 457
Wardziński, G., & Zdziarski, A. A. 2000, MNRAS, 314, 183
Zeiler, A., Biskamp, D., Drake, J. F., Rogers, B. N., Shay, M. A., & Scholer, M. 2002, J. Geophys. Res., 107, 1230
Zenitani, S., & Hoshino, M. 2001, ApJ, 562, L63